NACA

RESEARCH MEMORANDUM

ANALYTICAL AND EXPERIMENTAL STUDIES OF SPHERICAL SOLID-PROPELLANT ROCKET MOTORS

By Joseph G. Thibodaux, Jr., Robert L. Swain,
and George Wright

Langley Aeronautical Laboratory
Langley Field, Va.

NATIONAL ADVISORY COMMITTEE
FOR AERONAUTICS

WASHINGTON

August 16, 1957
Declassified March 18, 1960

NATIONAL ADVISORY COMMITTEE FOR AERONAUTICS

RESEARCH MEMORANDUM

ANALYTICAL AND EXPERIMENTAL STUDIES OF SPHERICAL SOLID-PROPELLANT ROCKET MOTORS

By Joseph G. Thibodaux, Jr., Robert L. Swain, and George Wright

SUMMARY

Analytical studies of spherical solid-propellant rocket-motor charge configurations have provided a basis for the design of a one-piece, case-bonded, radial-burning, three-dimensional, star-shaped charge which can be cast into a one-piece spherical shell. Experimental studies have provided techniques for the manufacture of spherical rocket motors incorporating this design. Successful static tests of three spherical rocket motors have demonstrated that a charge having a 95-percent volumetric loading factor, a variation from a mean value of surface area of less than ±10 percent, and a calculated sliver loss of 7 percent can be cast into a one-piece spherical shell. Performance estimates of conservative spherical rocket-motor designs using currently available propellants and conventional design techniques show that "vacuum velocities" in excess of 21,000 ft/sec can be attained by a one-stage spherical rocket motor.

INTRODUCTION

Recently, long-range ballistic missiles and satellites have been designed to fly trajectories in which at least one stage encounters little or no aerodynamic forces. The trajectory during firing of this stage is such that gravitational forces do not act in a manner which significantly reduces the velocity increment imparted by this stage below the calculated "vacuum velocity" increment. Under these conditions, the inherent shape of the rocket motor has no effect on the performance of the missile and conversely. If it can be assumed that the vacuum-velocity increment which can be imparted by this stage is the only criterion for evaluating rocket-motor performance, then the best rocket motor will be the one which gives the desired burnout velocity for the least-weight final stage. Other factors being equal, this will be the rocket motor which has the highest ratio of loaded weight to empty weight (mass ratio).

If the rocket-motor designer were asked to design a motor having the maximum possible mass ratio and if no restrictions were placed on its shape, he would undoubtedly consider a spherical design. It is well known that a spherical pressure vessel has the minimum weight for a given design volume and operating pressure. It can be shown that, for the same design conditions, a sphere weighs only three-fourths as much as an infinite cylinder and that additional weight is required to close the ends of the cylinder. A spherical rocket motor, therefore, should have the maximum possible mass ratio provided that a suitable charge design can be found and that techniques for manufacture of this rocket motor can be devised.

The problem of designing and manufacturing a spherical rocket motor presents many unique and difficult problems. In order for a spherical rocket motor to realize its potential advantages, internal ballistic characteristics of the spherical-charge design must be at least as good as those of the best available conventional-charge designs. Rocket-motor manufacturing techniques must be devised so that the advantages of a lightweight-shell design are not lost because of poor fabrication and assembly techniques or poor motor-operating characteristics. Analytical and experimental studies which led to the design and successful testing of a spherical rocket motor having excellent internal ballistic characteristics, and incorporating a one-piece spherical charge which can be cast into a one-piece spherical shell, are presented in this report.

SYMBOLS

A	cross-sectional area, sq in.
C_p	specific heat at constant pressure
C_v	specific heat at constant volume
C_p/C_v	ratio of specific heats
D	diameter of spherical charge, in.
F	thrust, lb
I_{sp}	specific impulse, lb-sec/lb
K	ratio of burning-surface area to throat area, S/A_t

k	propellant constant in burning-rate equation
M	molecular weight of rocket gases
N	number of segments
n	propellant exponent constant in burning-rate equation
R	radius, in.
r	propellant burning rate, in./sec
P	pressure, lb/sq in.
S	area of burning surface, D^2, sq in.
t	burning time, sec
ρ	density, lb/cu in.

Subscripts:

c	chamber
e	nozzle exit
t	throat
av	average
a,b,c,d,f,g,h, w,α,β,γ,η,δ	variables used in surface-area calculations defined in figure 15

Superscript:

*	estimated quantity

DESIGN AND ANALYSIS

Spherical-Charge Design

Desirable properties of any charge design are internal radial burning, a constant-burning surface, high volumetric loading, and low sliver loss. In addition, sufficient initial port area must be provided for unrestricted flow of burned propellant gases to the nozzle, and the structural design of the charge should be capable of withstanding all

forces which the rocket motor itself produces or is likely to encounter. In order to provide a basis for a spherical-charge design, the following characteristics were specified:

Loading density, percent	95
Burning-surface variation, percent	$< \pm 10$
Sliver loss, percent	<7

It was required that the charge be of the internal radial-burning type. The number of charge designs which might be considered are limited only by the imagination of the designer. In practice, the number of designs which will meet the required conditions is probably small.

Three general configurations were considered and all three could be designed to meet most of the conditions. Representative sketches of the three designs are shown in figure 1. The first case consisted of rotating stars with different numbers of points, angles, and diameters about the axis of the sphere. The second case consisted of conical and pyramidal projections on the inner surface of a hollow sphere ("Iron Maidens"). The third case, the one actually used, consisted of varying numbers of semicircular disks of different diameters which intersected along the axis of the sphere ("melon slices").

The first two cases had objectionable features. Large cantilevered propellant sections constituted a poor structural design and poor porting resulted in the flow meeting at the center of the sphere from many directions. The "melon slice" configuration appeared ideal for proper gas flow to the nozzle and was a good structural design for both axial and radial acceleration. The good porting of gases in this design should minimize internal-ballistic troubles resulting from erosion and pressure-drop considerations. For these reasons, only the melon-slice configuration was completely analyzed. Designs consisting only of disks which intersected along the axis of the sphere gave excessive sliver loss. This loss was easily remedied by placing integral ring segments at the perimeter of the disks to give a "double web" design. Details of the analysis and sample calculations are presented in the appendix. Three views of a typical case mandrel designed by using the methods presented in the appendix are shown in figure 2. It should be noted that the charge is what remains if this mandrel were melted out of a sphere of propellant whose diameter is 10/7 the diameter of the mandrel. A cross section of a plane through the equator of a mandrel for a 10-inch-diameter spherical rocket motor is shown in figure 3. Based on this design, calculations for the variation of propellant burning-surface area as a function of web fraction burned were made and are presented in figure 4. These calculations show that the burning-surface variation from a mean value of 360 square inches is less than ±10 percent.

Internal Ballistics and Operating Characteristics of Rocket Motor

In order to demonstrate that the spherical charge as designed was practical, it was necessary to design an actual rocket motor utilizing this charge. The following internal ballistics and operating characteristics of the rocket motor were arbitrarily specified:

Operating pressure, lb/sq in.	500 to 1,000
Burning time, sec	<5
Diameter, in.	10

These characteristics of the charge, coupled with the web dimensions (1.5 inches) and burning-surface area (360 square inches), were used to select a propellant. It was decided to use the Thiokol T-21 polysulfide-perchlorate formulation as this propellant is easy to mix (batch) and cast, gives good performance, is within the specified burning time over the entire operating-pressure range, and has a low pressure exponent n. Based on the parameters of the spherical-charge design and the T-21 propellant characteristics as obtained from reference 1, the following internal ballistics and operating characteristics of the rocket motor were obtained or calculated for an operating pressure of 1,000 lb/sq in.:

K	260
r, in./sec	0.513
I_{sp}, lb-sec/lb	206
n	0.303
C_p/C_v	1.24
M (molecular weight)	25.7
S, sq in.	360
A_t, sq in.	1.38
A_e/A_t	8.1
t, sec	2.92
F_{av}, lb	1,945
Motor-propellant quantity, lb	29.8

Shell Design

No attempt was made to design or construct a lightweight shell for the initial spherical-rocket-motor tests. A spherical shell having a 10-inch inside diameter was fabricated from two hemispheres spun of SAE 4130 steel having a nominal thickness of 1/16 inch. During the spinning process the wall was thinned to 0.040 inch in some places. The rear half of the shell was reinforced to provide for nozzle attachment and to withstand heating as the propellant burned and exposed the

shell to hot propellant gases. The two hemispherical shells were welded to heavy flanges which allowed easy assembly and disassembly for reuse after each test. A drawing of the assembly of the motor shell and nozzle is shown in figure 5. Views of the front and rear shell halves are shown in figure 6. In actual practice it should not be difficult to join the shell halves by welding.

Mandrel Design

The mandrel was constructed of seven semicircular disks with integral ring segments at the perimeter of the disks as shown in figures 2 and 3. These disks were cast in one piece about a central core. The mandrel was fitted with a shank which was used to aline and support it in the spherical shell during casting and curing as shown in figures 2 and 7.

The mandrel was cast of "Cerrobend" (an eutectic alloy of lead, tin, bismuth, and cadmium) which melts at 158° F. The mandrel remains solid during the cure and is easily melted out by elevating the temperature to 165° F.

EXPERIMENTAL RESULTS

Mixing, Casting, and Curing

Conventional methods were used in mixing the propellant. For casting, the mandrel was threaded and mounted to the rear half of the shell as shown in figure 7. The shell halves were bolted together, set upright, and the viscous propellant was pumped into the rocket shell through the holes in the mandrel support as shown in figure 7(b). The propellant was then cured for 4 days at a temperature of 150° F.

After curing, the shell was inverted and the oven temperature was raised to 165° F. Most of the mandrel melted and flowed out, leaving the propellant surface covered with a thin film of alloy. This film was removed by filling the cavity with mercury to dissolve the alloy. When the mercury was poured out, a perfectly clean propellant surface remained. The completed rocket motor is shown in figure 8.

Because it was believed that the curing exotherm might cause premature melting of the mandrel, initial mandrels were made of an eutectic alloy of lead, bismuth, and cadmium which melts at 196° F. Removal of this alloy was difficult, and temperatures necessary to effect removal resulted in damage to the propellant.

The first rocket motor was cast and cured with no trouble. During the cure of the second rocket motor, melting of the mandrel support shank resulted although proper oven temperatures were indicated. The mandrel dropped and thus decreased the front web to approximately 3/4 inch. It is felt that the melting was due both to faulty oven controls and to the temperature rise resulting from the additional heat input of the propellant-curing exotherm.

For the third rocket motor a temperature control was maintained on the rocket shell itself. During the first day, both the oven and the shell remained at 150° F. After the first day the control system reduced the oven temperature and varied it between 125° F to 135° F for the rest of the time while maintaining the shell at the desired 150° F. Smaller test motors using the same propellant were in the oven at the same time and were uncured even though the large motor was completely cured.

Static Tests and Results

Propellant test motors.- It was to be expected that the propellant manufactured at the Langley Aeronautical Laboratory would differ in performance and ballistic characteristics from the Thiokol T-21 propellant because of lack of quality control for grinding and mixing. A series of three cylindrical test motors, 3 inches in diameter by 5 inches long, were cast from each batch of propellant and were cured with each spherical rocket motor. These motors were then fired at chamber pressures of approximately 500, 1,000, and 1,500 lb/sq in. to establish ballistic characteristics for each batch of propellant. Plots of K (ratio of burning-surface area to throat area) as a function of pressure were then made as shown in figure 9 to give a comparison of the standard T-21 propellant with the type manufactured at Langley. No data were available for the second spherical rocket motor because all the test motors failed. These failures resulted from an error in machining the test-motor headcaps. A study of the initial portion of each firing record prior to failure did not indicate that the propellant was at fault.

Normally, the test motors would be fired and the ballistic properties of the propellant would be established before machining the final spherical-rocket throat diameter to give the proper operating pressure for the particular batch. In the interest of saving time, all nozzles were machined to a specified diameter before the propellant was cast. Static tests were then made and the measured values compared very well with the predicted values on the basis of actual propellant batch ballistics.

Motor mounting.- All the spherical motors were mounted in a large cylindrical pipe. This pipe was mounted on the vee-rollers of the thrust stand and were butted against a strain gage which measured the thrust

output of the motor as shown in figure 10. In addition, chamber pressures were measured on the second and third firings.

Igniter.- The igniter was fabricated from thin gauze strips which were impregnated with a mixture of magnesium powder, potassium perchlorate, Vistanex, and toluene. The impregnated gauze strips were inserted into the tee-flares along the outer perimeter of each segment. Two match squibs, connected by a 4-inch-long, 1/4-inch-diameter, cellophane tube filled with 3 grams of FFFG black powder, were used to ignite these gauze strips. A 1/16-inch-thick plastic blowout disk was cemented in the throat to build up operating pressure quickly; smooth ignition was obtained in all three firings.

Test results.- The results of firing of the three spherical rockets are shown in figures 11, 12, and 13 and are listed in table I. The chamber pressure shown in figure 11 was calculated from the thrust record.

The design pressure for all three rocket motors was 1,000 lb/sq in. The throat and exit diameters were based on the ballistic characteristics of the T-21 propellant. As indicated by curve (a) of figure 9(a), the ballistic properties of the batch of propellant used in the first spherical rocket motor were different from those assumed and a value of $K = 260$ would be expected to yield a chamber pressure of 665 lb/sq in. gage. The calculated chamber pressure as shown in figure 11 was 635 lb/sq in. gage. Since the nozzle was designed for optimum expansion from 1,000 lb/sq in. to sea-level atmospheric pressure, the gases were overexpanded for the first firing. A neutral thrust-time history with an acceptable amount of "tail-off" was obtained on firing spherical rocket 1 as shown in figure 11. The combustion was smooth with no evidence of resonance. A total impulse of 5,786 lb-sec was obtained which gave a propellant specific impulse of 194 lb-sec/lb. An average thrust of approximately 1,350 pounds for a duration of 4 seconds was obtained.

Although the web at the head end of spherical rocket motor 2 was reduced to 3/4 inch because of melting of the mandrel as mentioned earlier, it was felt that the propellant charge was not sufficiently deformed to warrant canceling the test. The rocket motor was fired and operated smoothly yielding a long tail-off as shown in figure 12 as would be expected from an off-center core. The motor gave a total impulse of 5,566 lb-sec and a propellant specific impulse of 186 lb-sec/lb.

Excellent results were obtained from the firing of spherical rocket motor 3. The thrust time history as shown in figure 13 was similar in shape to the area curve predicted in figure 4. The combustion was smooth with the deviation from predicted values due principally to different ballistic characteristics of the propellant batch as shown in figure 9(b). The large hump in thrust is due to a higher value of n, the exponent in

the burning-rate equation $r = kP_c^n$. This gave a total impulse of 6,030 lb-sec with a propellant specific impulse of 202 lb-sec/lb.

DESIGN AND PERFORMANCE CALCULATION OF 20-INCH SPHERICAL ROCKET MOTOR

It is assumed that a spherical shell can be fabricated from conventional materials and that the ratio of design stress to working stress is 1.5, a conservative number for high-performance rocket-motor shells by current standards. The operating pressure will be 600 lb/sq in. at 70° F. The shell is to be fabricated from heat-treated stainless steel having a minimum yield stress of 210,000 lb/sq in. and a density of 0.282 lb/cu in. The propellant is assumed to have a specific impulse of 227 lb-sec/lb at the specified operating pressure which expanded to sea-level atmosphere pressure. The propellant density is 0.0635 lb/cu in., the burning rate is approximately 0.4 in./sec, and the pressure exponent n is approximately 0.3.

The basic spherical-shell weight is 8.16 pounds. If 0.8 pound is allowed for additional thickness at the welded joint and for nozzle-attachment fitting, the entire shell weight is 8.96 pounds. The total propellant weight is 251 pounds. This value will be decreased to 250 pounds to allow for a liner and insulation at the nozzle approach. The thrust of the rocket will be approximately 8,100 pounds. The burning time will be approximately 6.5 seconds. It should be possible to fabricate a nozzle for this thrust and duration for a weight of 6 pounds. If 1 pound is allowed for liner and insulation, the total inert weight will be 16 pounds, and the total loaded weight will be 266 pounds. The motor will have a mass ratio of 16.6 and a ratio of impulse to weight of 213 lb-sec/lb loaded weight. This motor, if launched at an altitude sufficiently high to neglect drag, would give an incremental velocity of 21,700 ft/sec, and with an 8-pound payload, would give an incremental velocity of 18,600 ft/sec. By using lower operating pressures, higher specific-impulse propellants, denser propellants, or less conservative design, even higher ratios of impulse to weight, mass ratios, and higher attainable incremental velocities can be realized.

CONCLUDING REMARKS

Techniques for the design and fabrication of a spherical rocket motor incorporating a one-piece castable propellant charge having an intricate core configuration in a one-piece spherical shell have been successfully devised and demonstrated.

The charge design gives internal ballistics and operating characteristics which are comparable with those of the best rocket motors of conventional design.

A spherical rocket motor, by virtue of its high loading density and efficient pressure vessel design, should allow an appreciable increase in the performance of solid-propellant rocket motors.

These same design and fabrication techniques open up new avenues of possibilities to charge designers and will allow design and fabrication of new rocket-motor shapes.

Design and construction of spherical solid-propellant rocket motors capable of achieving single-stage "vacuum velocity" increments greater than 21,000 ft/sec appear to be feasible by utilizing currently available propellants and fabricating techniques.

Langley Aeronautical Laboratory,
National Advisory Committee for Aeronautics,
Langley Field, Va., July 10, 1957.

APPENDIX

CALCULATION OF INTERNAL BURNING-SURFACE AREA

Because of the complex nature of the anticipated internal port configuration, an approximate method was used to calculate the internal burning-surface area S as a function of burning time. No attempt was made to calculate this area by exact methods. The method utilized was partly numerical and partly graphical. Small curved surfaces with large radii of curvature were assumed planar. A correction factor was applied to larger curved areas calculated by planar formulas.

The design specifications stated a minimum volumetric loading density of 95 percent with a maximum sliver of 7 percent. The thrust time history was to be neutral with little tail-off. The burning-time specification was sufficiently long to avoid being a design consideration. It was decided that the general design would entail a number of semicircular segments (melon slices) fitted about a central cylinder. Calculations were made to determine the effect of varying the web thickness, number of segments or slices, and thickness of segments on surface area, loading density, and sliver. See figure 14 for the internal configuration and nomenclature for design calculations.

Preliminary calculations were carried out for $N = 6$, 7, and 8; $w = 0.05D$ to $0.20D$; and a thickness range from 0 to $0.12D$. Excessive sliver loss eliminated the design with $N = 6$, whereas low loading density eliminated the design with $N = 8$. All further calculations were limited to the design with $N = 7$ even though the preliminary design for $N = 7$ failed to meet the specifications. A tee-flare (as shown in fig. 3) replaced the thin, square rim, and the whole segment was tapered to increase the loading density. Calculations of S were performed at burning intervals of $w/6$. A sample calculation is presented subsequently.

The total burning-surface area was calculated in portions. The calculation of the initial burning-surface area is presented here. Figure 15 presents sketches used in the computations.

Portion 1

The facial area of each melon slice of propellant from the intersection of facial area planes to the intersection of these planes with the start of the tee-flare at the rim of the segment is portion 1. The desired area is shaded in figure 15(b). By referring to figures 15(a) and 15(b), it is seen that

$$b \eqsim \overline{Oc}$$

$$a = 0.125 \text{ inch}$$

$$\alpha = 25.7^\circ$$

and

$$b = \frac{a}{\tan \alpha} = \frac{0.125}{0.48127} = 0.2597 \text{ inch}$$

Therefore, the area of the shaded portion is given by

$$A_1 = \int_0^r \int_0^{\sqrt{r^2-x^2}} dy\, dx - \int_0^{0.2596} \int_0^{\sqrt{r^2-x^2}} dy\, dx$$

$$= \frac{\pi r^2}{4} - \left[\frac{1}{2}\left(x\sqrt{r^2 - x^2} + r^2 \sin^{-1}\frac{x}{r}\right)\right]_0^{0.2596}$$

With $r = 3.3$ inches, the total facial area of portion 1 becomes

$$A_{1,\text{total}} = 28(8.553 - 0.855) = 215.54 \text{ square inches}$$

Portion 2

The flat portion on the under side of the tee-flare along the perimeter between the intersection of adjacent segments (portion d in fig. 15(c)) is portion 2. In order to determine the approximate perimeter, it was necessary to calculate the quantity h in figure 15(d) with the aid of figure 15(a). Thus, if

$$a = 0.375 \text{ inch}$$

and

$$b = \frac{0.375}{0.48127} = 0.7792 \text{ inch}$$

then

$$b \eqsim h$$

With g estimated to be 3.47 inches,

$$\tan \gamma = \frac{h}{g}$$

$$\gamma = \tan^{-1} \frac{0.7792}{3.47} = 12.67^\circ$$

$$\text{Perimeter angle} = \eta = 180^\circ - 2(12.67^\circ) = 154.66^\circ$$

$$\text{Perimeter} = \frac{\pi g \eta}{180^\circ} = \frac{(\pi)(3.35^* \text{inches})(154.66^\circ)}{180^\circ} = 9.036 \text{ inches}$$

Therefore, the total facial area of portion 2 becomes

$$A_{2,\text{total}} = 14\left[(\text{Perimeter})(d^*)\right]$$

$$= 14\left[(9.036)(0.29)\right] = 36.69 \text{ square inches}$$

Portion 3

The circular portion on the rim of the tee-flare along the perimeter between the intersection of adjacent segments (arc subtended by β in fig. 15(c)) is portion 3. The perimeter will be the same as that determined in portion 2 and β is read from figure 15(c). Thus,

$$\beta = 153^{\circ *}$$

$$f^R = 0.05 \text{ inch}$$

The arc subtended by β is given by

$$\beta = \frac{153}{360} 2\pi f^R$$

$$= \frac{153}{360} (2\pi)(0.05) = 0.1335 \text{ inch}$$

Therefore, the facial area of portion 3 becomes

$$A_3 = 14\left[(\text{Perimeter})(\text{Arc of } \beta)\right]$$

$$= 14\left[(9.036)(0.1335)\right] = 16.89 \text{ square inches}$$

Portion 4

The flat rim of the tee-flare along the perimeter between the intersection of adjacent segments (0.65 inch in all cases) is portion 4. The perimeter is approximately that used in portions 2 and 3. Therefore, the facial area of portion 4 becomes

$$A_4 = 7\left[(\text{Perimeter})(0.65)\right]$$

$$= 7\left[(9.036)(0.65)\right] = 41.11 \text{ square inches}$$

Portion 5

The front end which is a seven-sided polygon with length l of each side equal to 0.65 inch is known as portion 5. The area of portion 5 becomes

$$A_5 = 3.63391\, l^2$$

$$= (3.63391)(0.65)^2 = 1.54 \text{ square inch}$$

The rear end is the port area.

Portion 6

Small triangles known as portion 6 are formed by the flat portion along the under side of the tee-flare from the intersection of adjacent segments along the intersection of the aforementioned flat portions. These areas will be only approximated. With

$$\text{Altitude} \approx 0.7792 - 0.2596 = 0.5196 \text{ inch}$$

and

$$\text{Base} \approx 0.3 \text{ inch}$$

the area of portion 6 having 28 triangles is

$$A_6 \approx (28)\,\frac{1}{2}\,(\text{Altitude})(\text{Base}) = (28)\,\frac{1}{2}\,(0.5196)(0.3) = 2.18 \text{ square inches}$$

For all calculations, the port area is assumed inhibited or not susceptible to burning.

Total Burning-Surface Area of Portions

The total burning-surface area of all six portions is found to be 313.95 square inches. The difference between the calculated result here and the initial burning-surface area from figure 4 is due to the slightly different configuration used for the calculation of figure 4. A mean surface area of 360 square inches was used for the calculation of the interior ballistics of the spherical rocket motor.

REFERENCE

1. Anon.: Propellant Powder Manual. SPIA/M2 (Contract NOrd 7386), The Johns Hopkins Univ., Appl. Phys. Lab., Jan. 1957.

TABLE I

FIRING TEST DATA OF 10-INCH SPHERICAL ROCKET MOTOR

Spherical rocket motor	Date fired in 1957	Approximate propellant temperature, °F	Total impulse, lb-sec	Charge weight, lb (a)	Propellant impulse, lb-sec/lb
1	Jan. 18	65	5,786	29.77	194
[b] 2	Feb. 21	76	5,566	29.85	186
3	May 8	75	6,030	29.80	202

[a] T-21 type propellant used for all tests.

[b] Slightly disfigured charge due to partial mandrel melting during curing process.

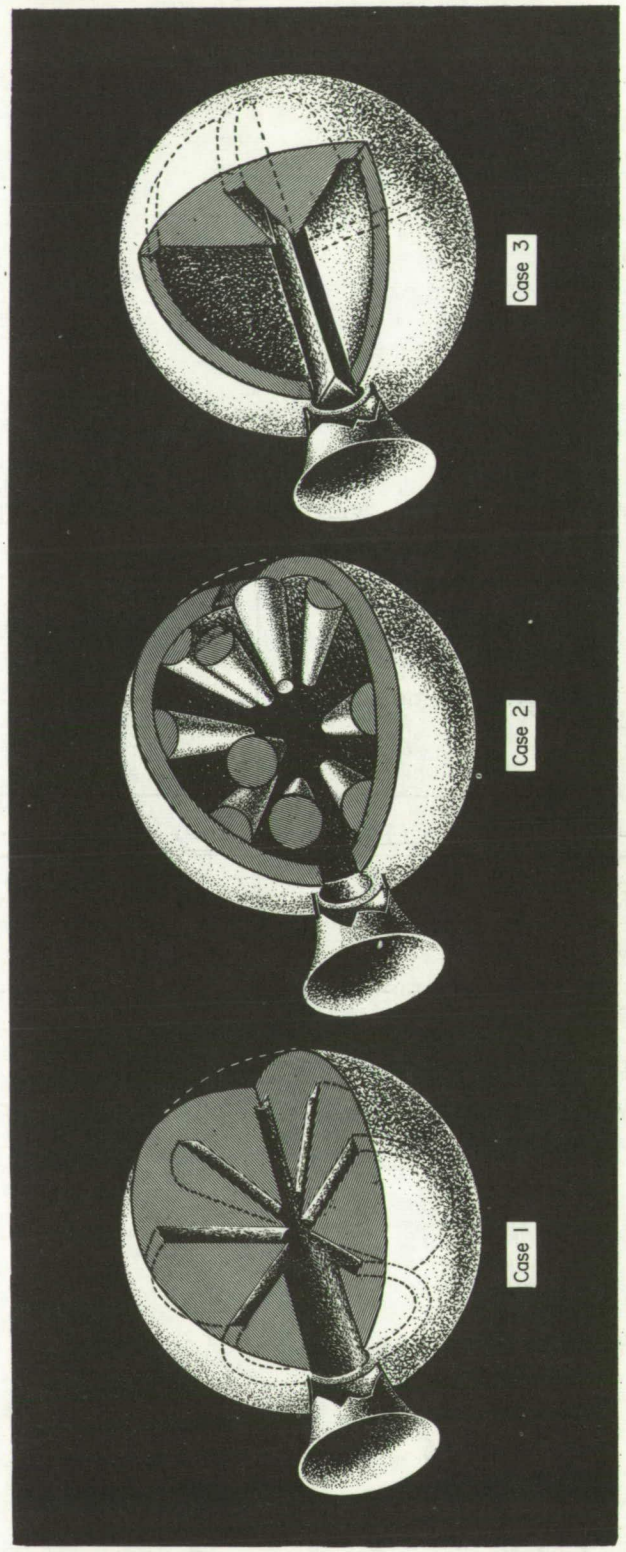

Figure 1.- Three sperical internal configurations considered in analysis.

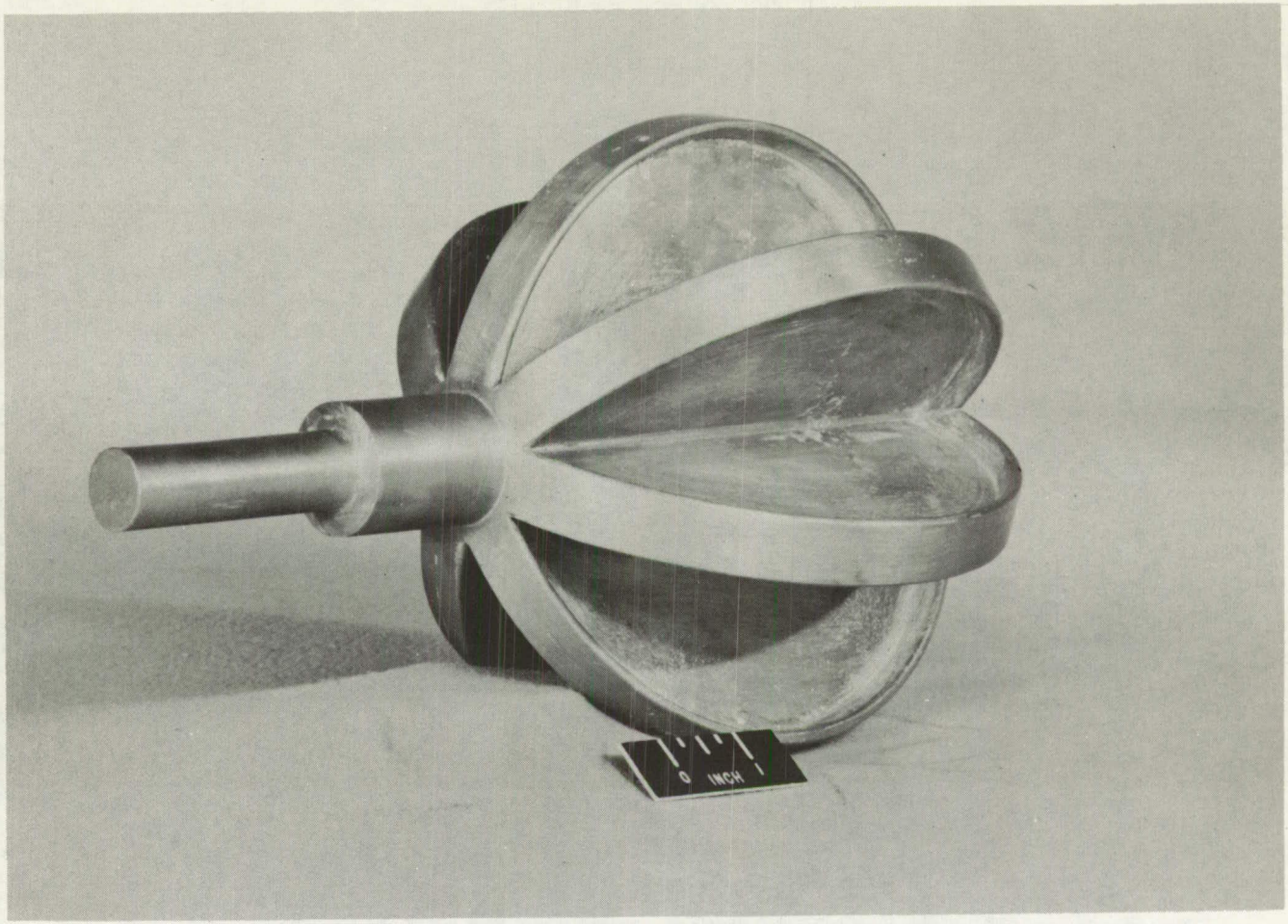

(a) Side-rear view. L-57-275

Figure 2.- Port-cavity mandrel.

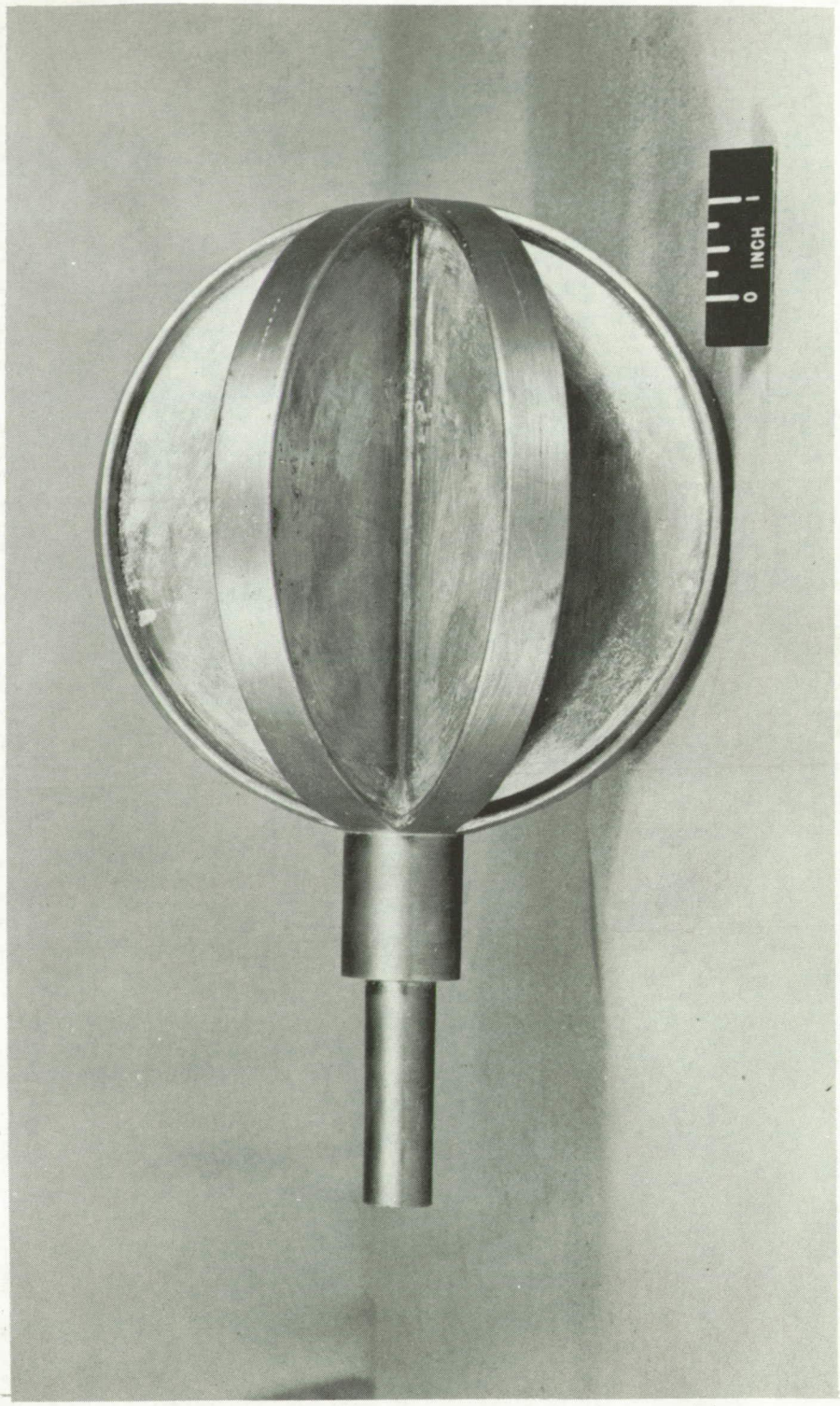

L-57-273

(b) Side view.

Figure 2.- Continued.

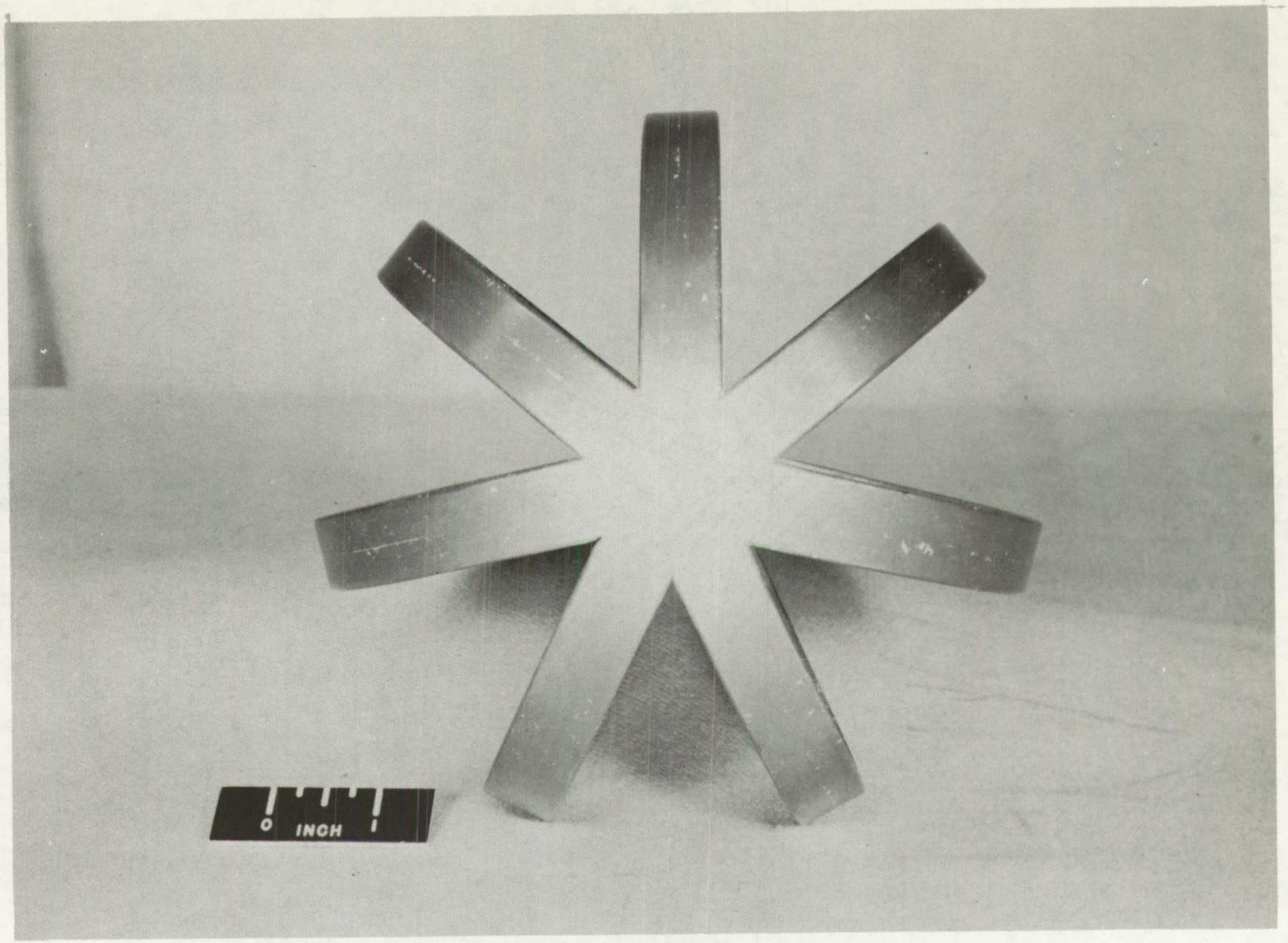

(c) Front view. L-57-274

Figure 2.- Concluded.

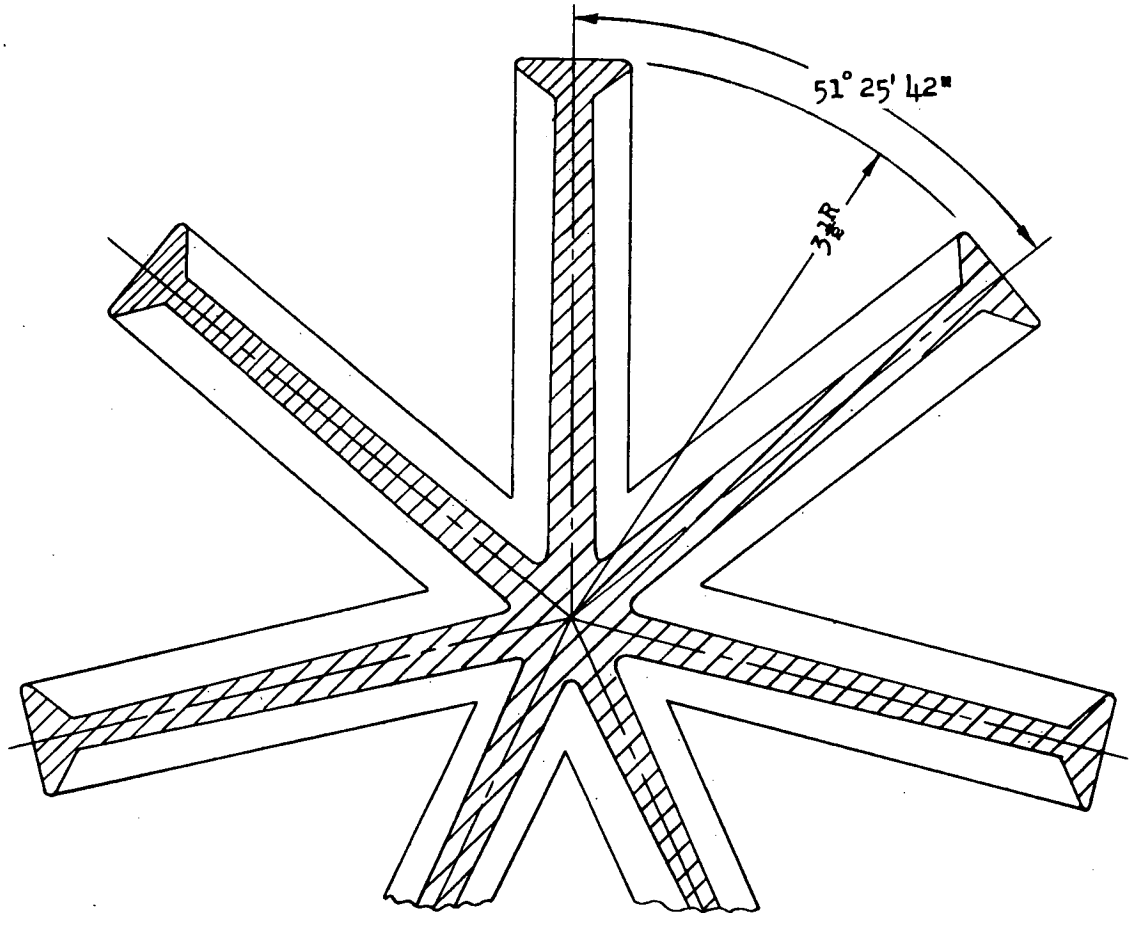

(a) Full axial section at center of sphere.

(b) Typical segment.

Figure 3.- Cross section of port-cavity mandrel configuration. All dimensions are in inches unless otherwise specified.

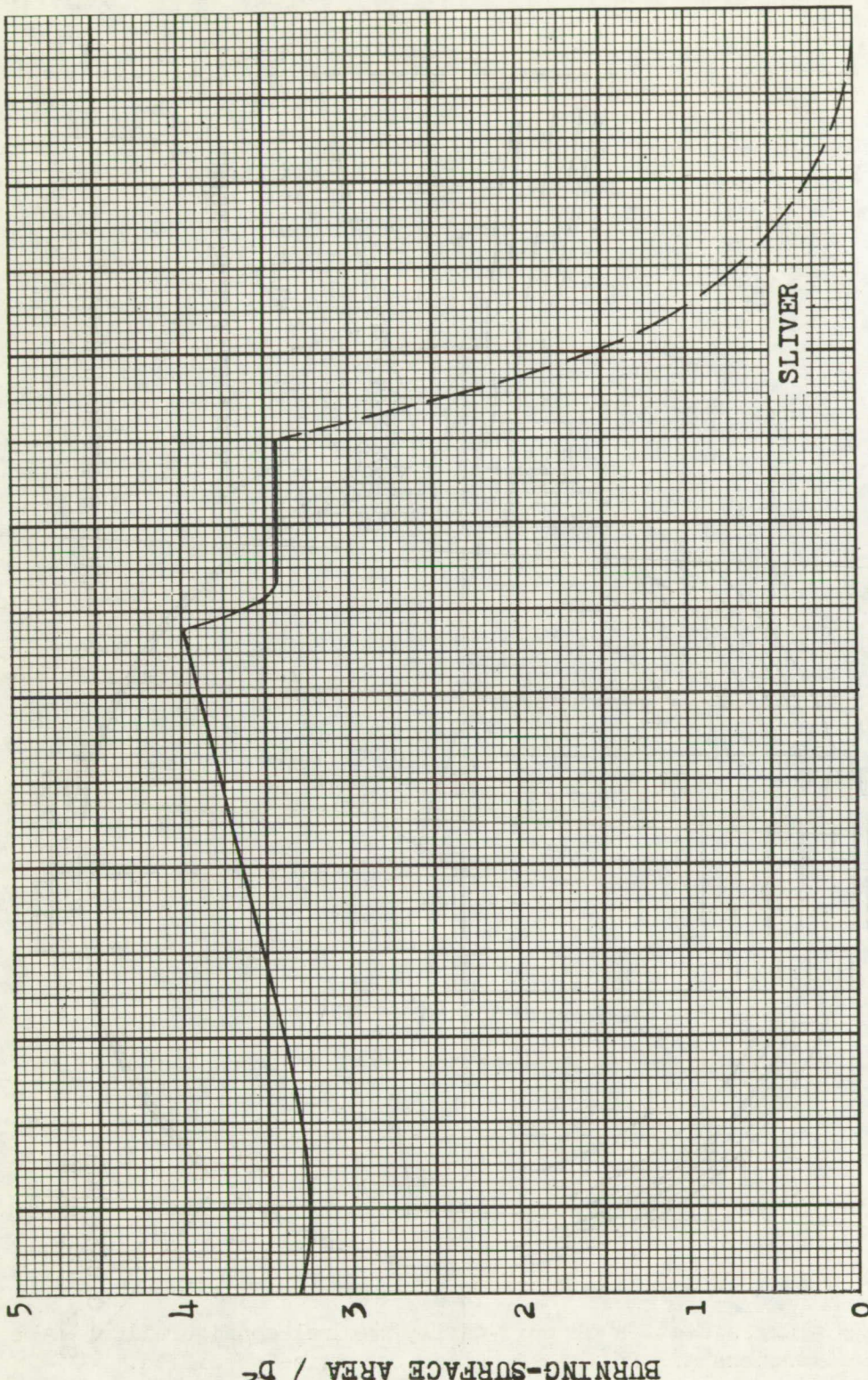

Figure 4.- Calculated burning-surface area for final configuration.

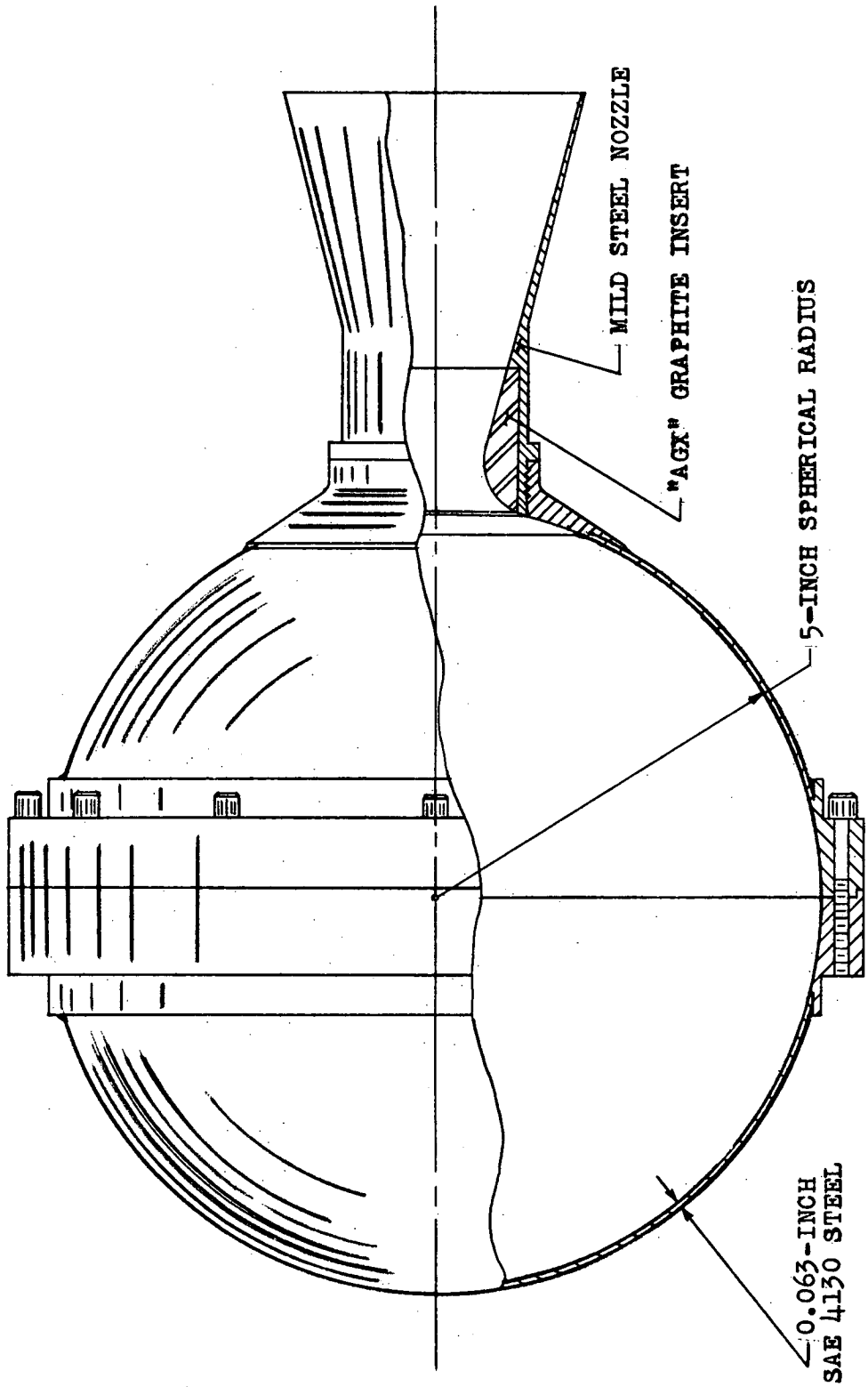

Figure 5.- Static test case of 10-inch spherical rocket motor.

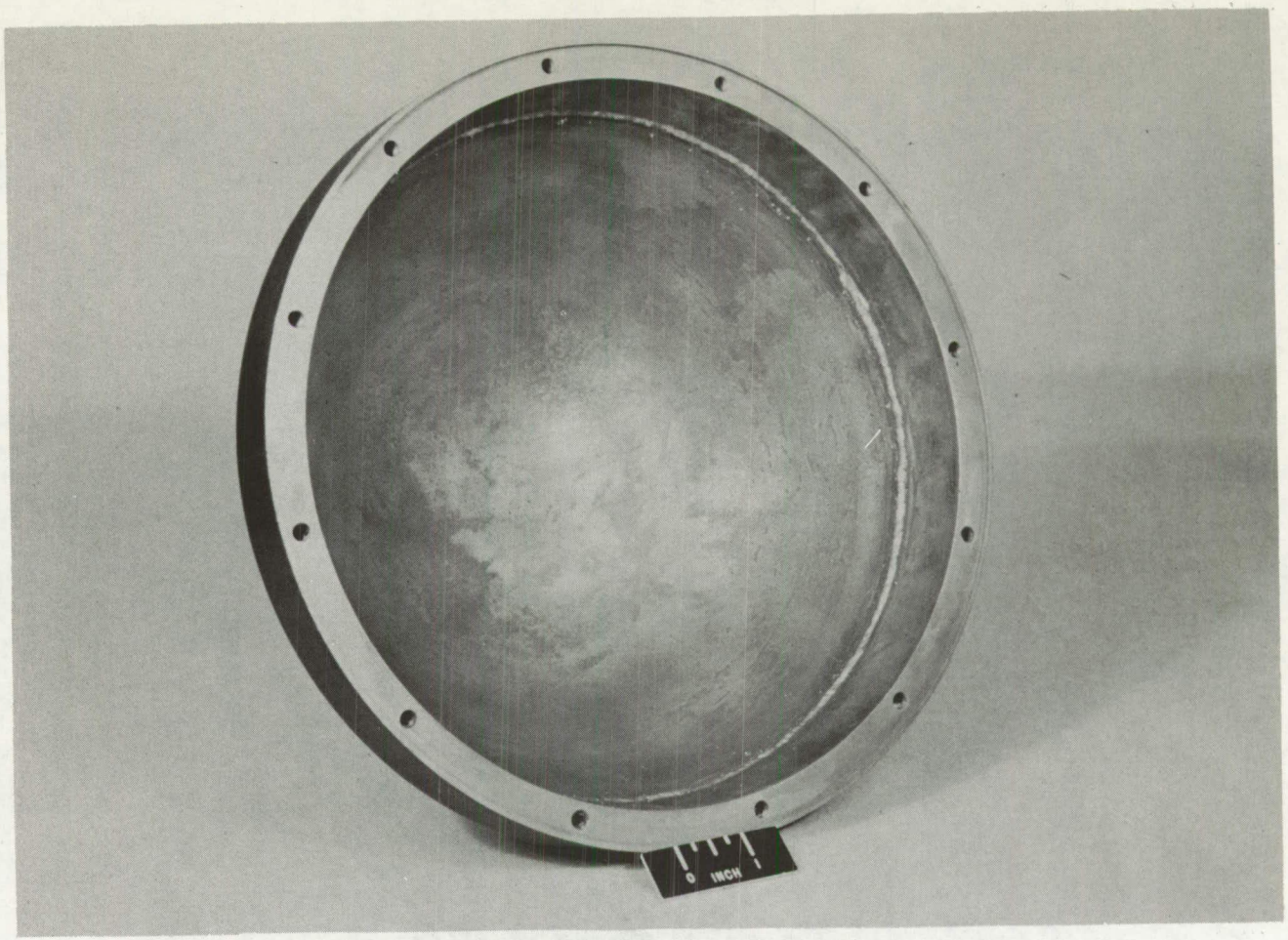

(a) Front half. L-57-272

Figure 6.- 10-inch spherical rocket shell.

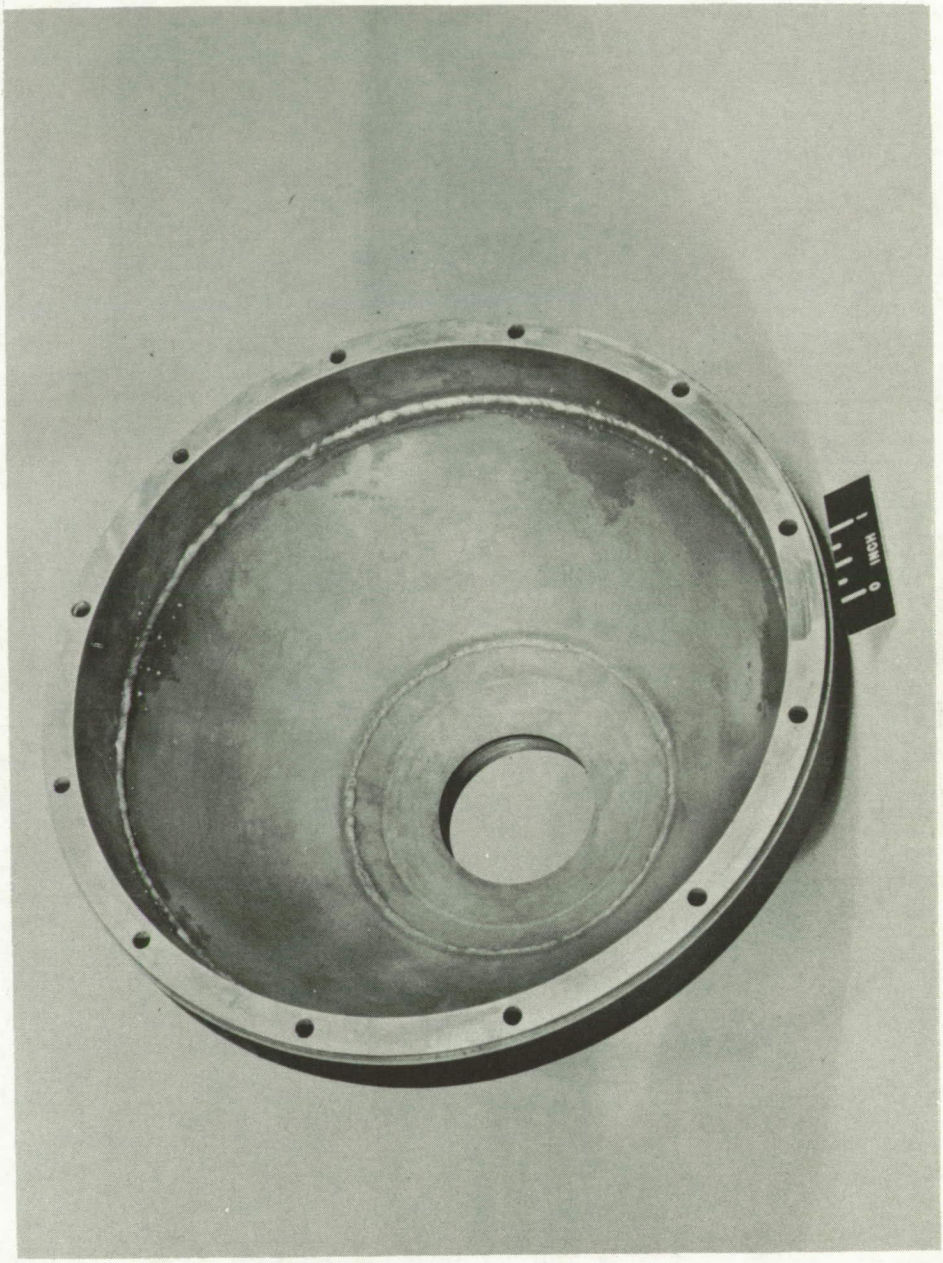

L-57-271

(b) Rear half.

Figure 6.- Concluded.

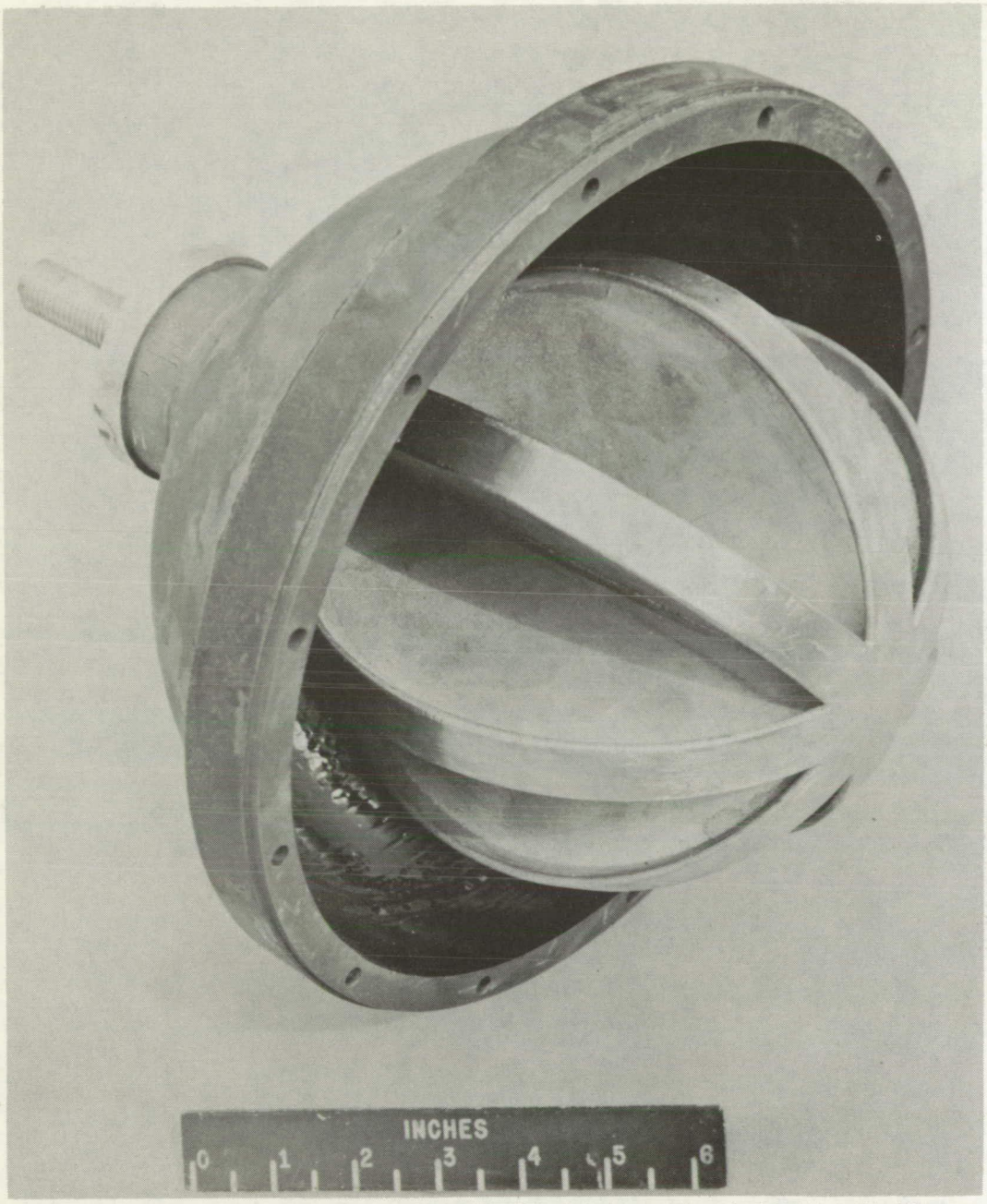

(a) Side-front view. L-57-1752

Figure 7.- Port-cavity mandrel mounted to rear half of case for casting.

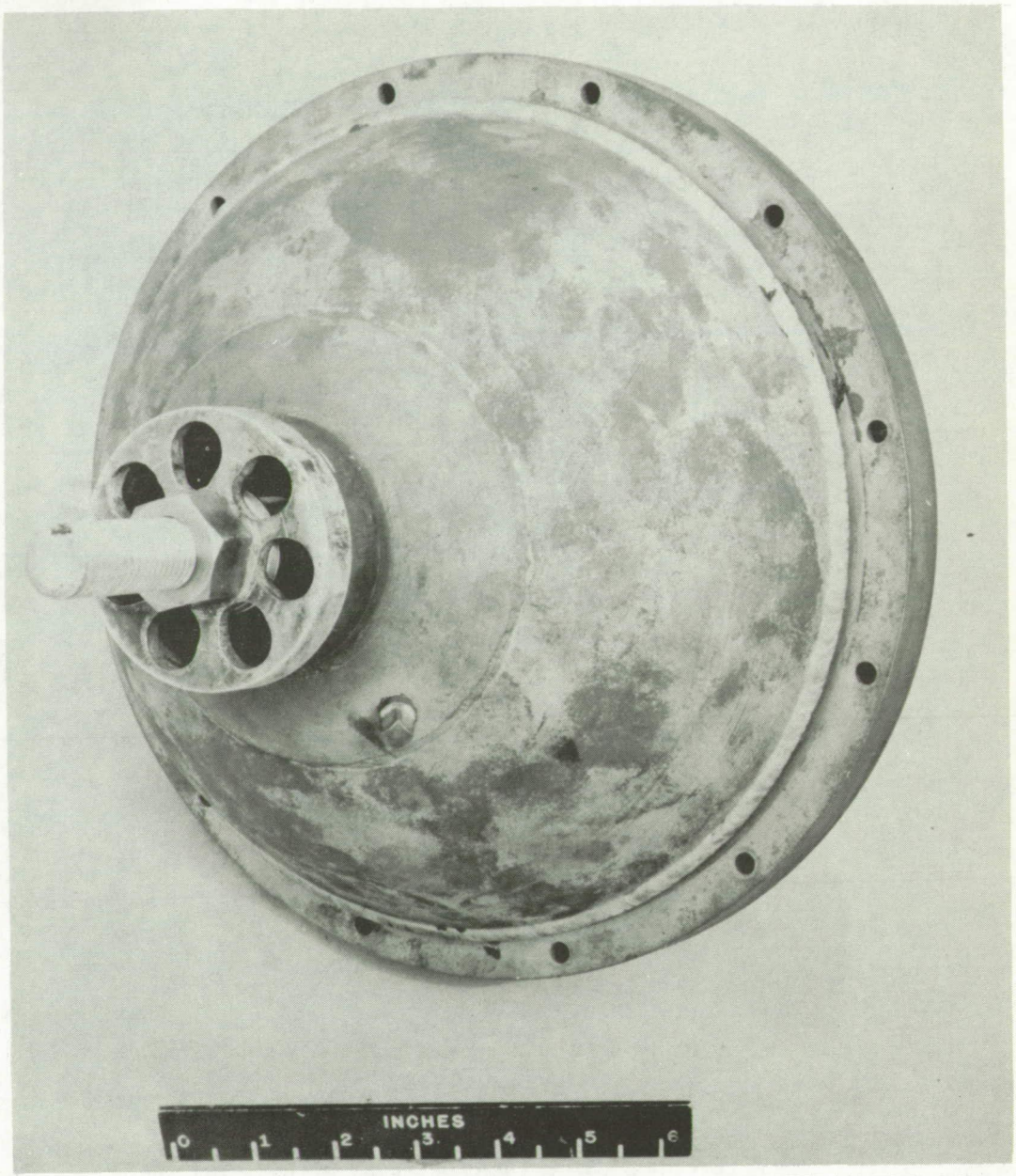

(b) Side-rear view. L-57-1753

Figure 7.- Concluded.

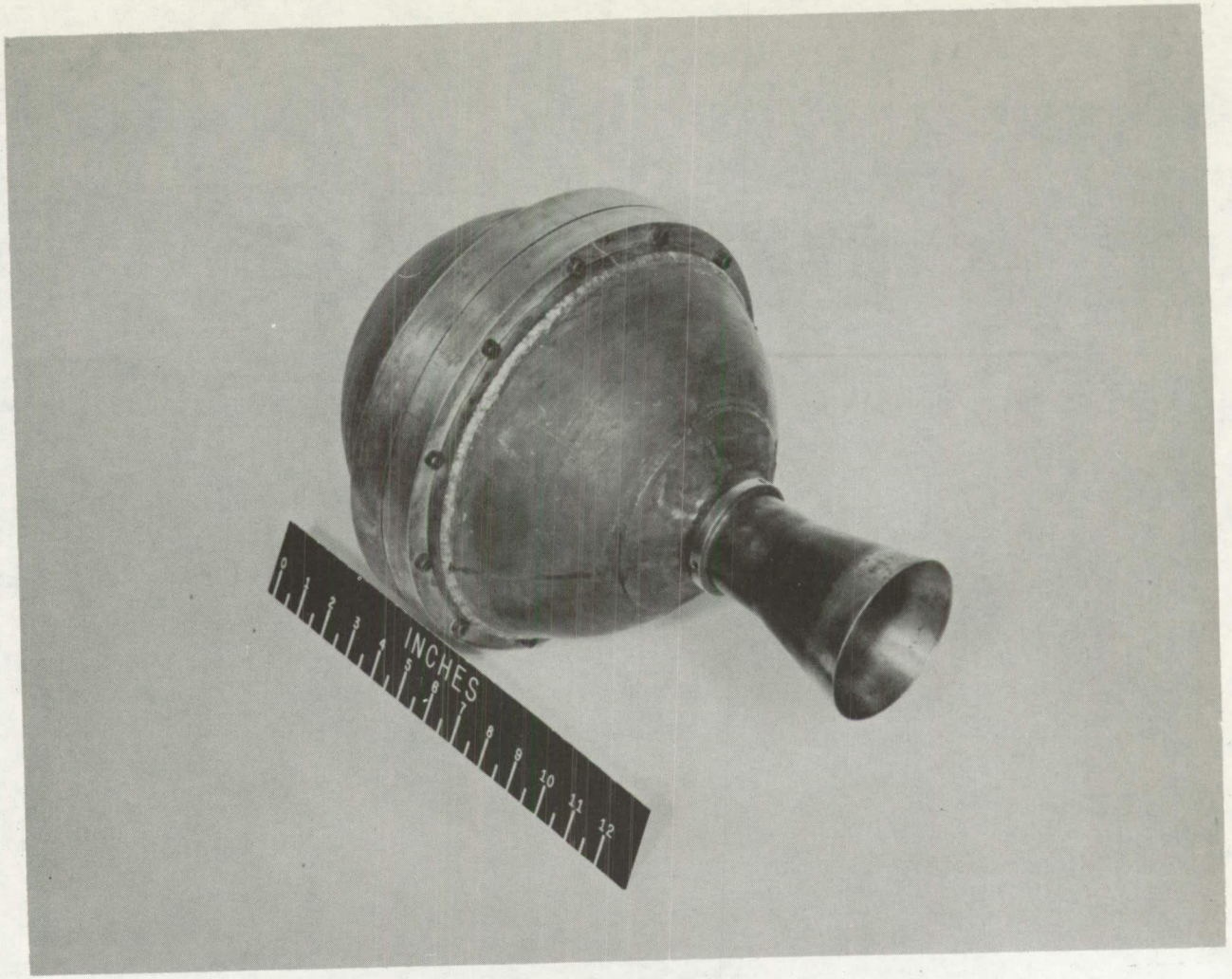

(a) Side-rear view. L-57-225

Figure 8.- 10-inch spherical rocket motor.

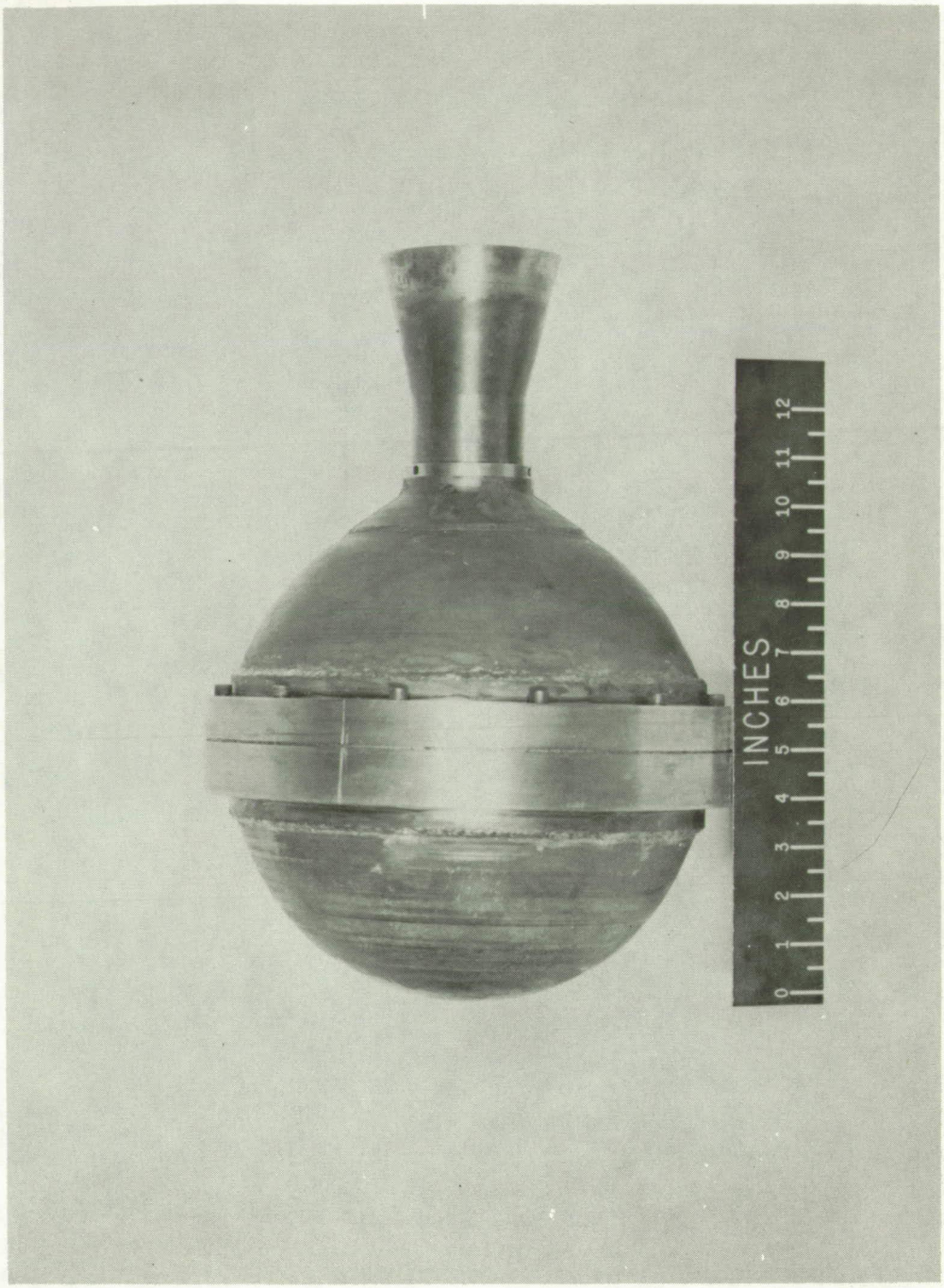

L-57-226

(b) Side view.

Figure 8.- Continued.

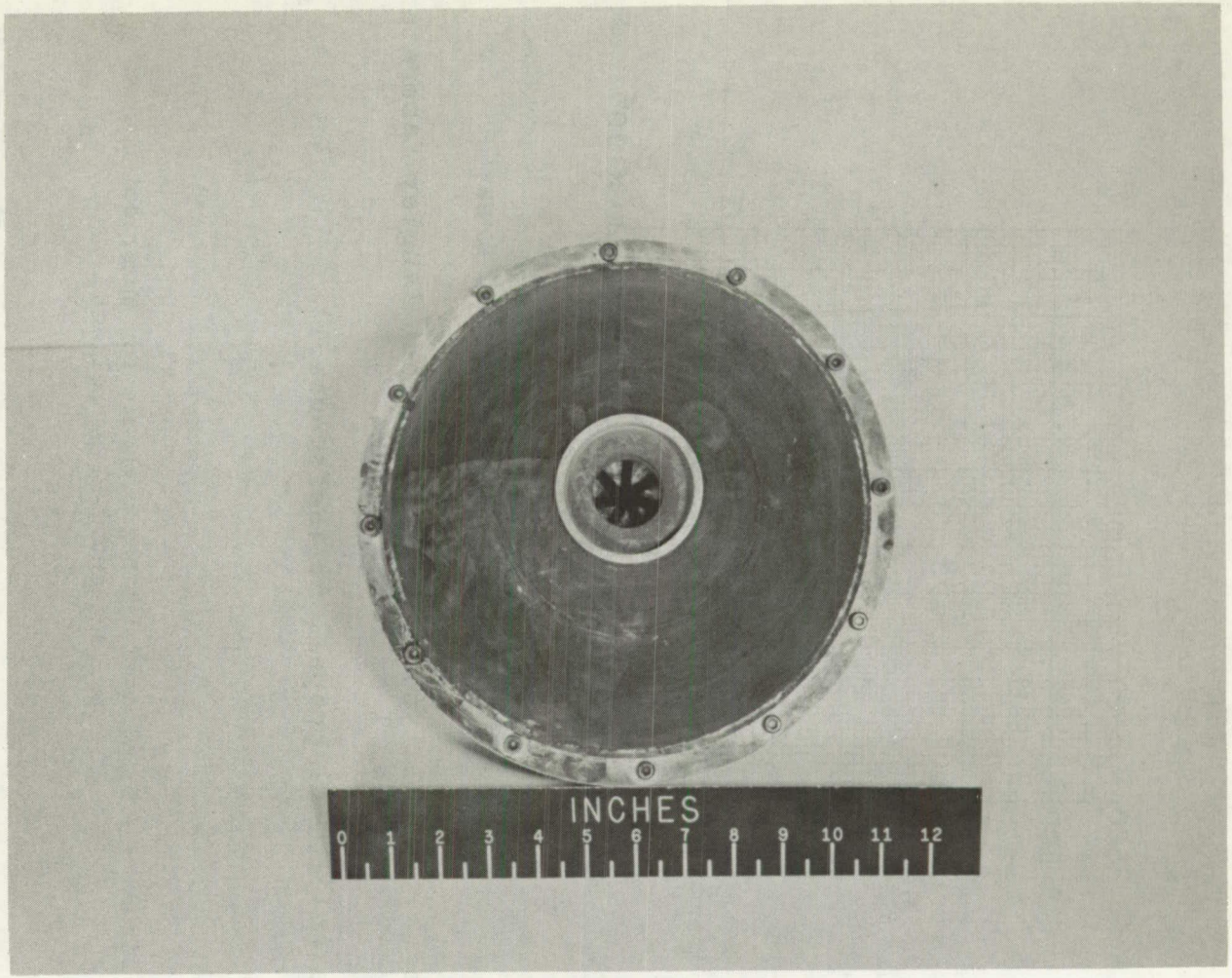

(c) Rear view without nozzle. L-57-228

Figure 8.- Concluded.

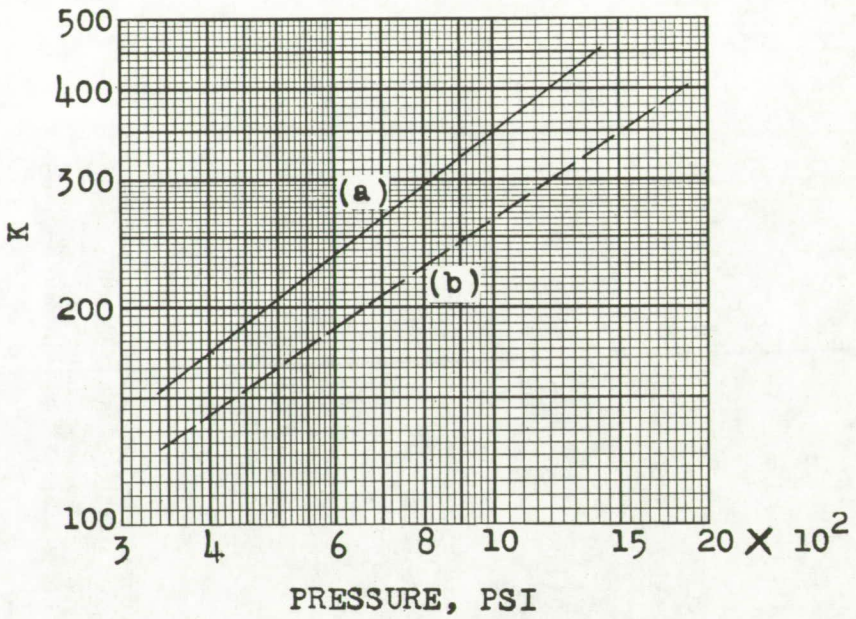

K = Burning-surface area / Throat area

Curve (a) : T-21 type propellant cast at Langley Laboratory (No. 1 spherical rocket)

Curve (b) : T-21 propellant (Reference 1)

(a) Spherical rocket 1.

Figure 9.- K plotted against pressure for spherical-rocket propellant and T-21 propellant.

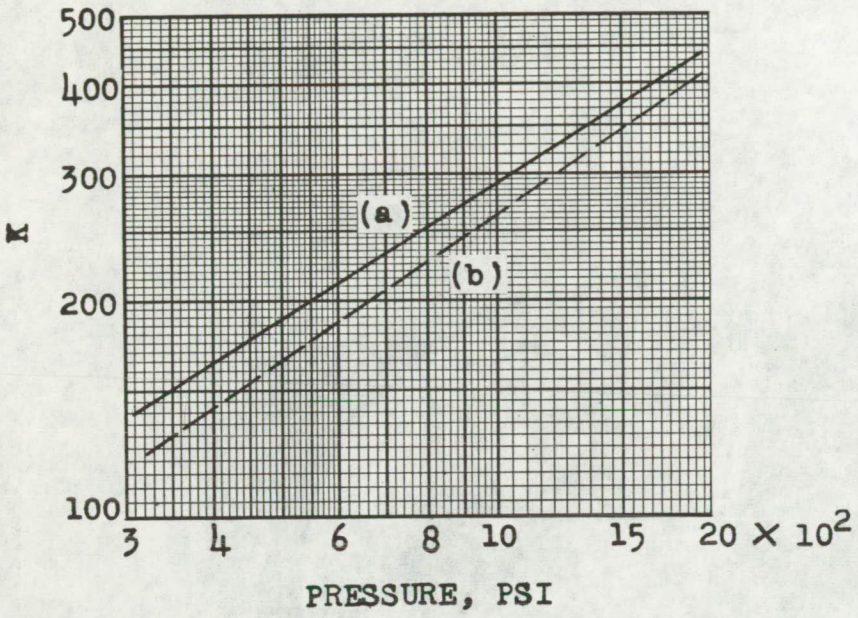

K = Burning-surface area / Throat area

Curve (a) : T-21 type propellant cast at Langley Laboratory (No. 3 spherical rocket)

Curve (b) : T-21 propellant (Reference 1)

(b) Spherical rocket 3.

Figure 9.- Concluded.

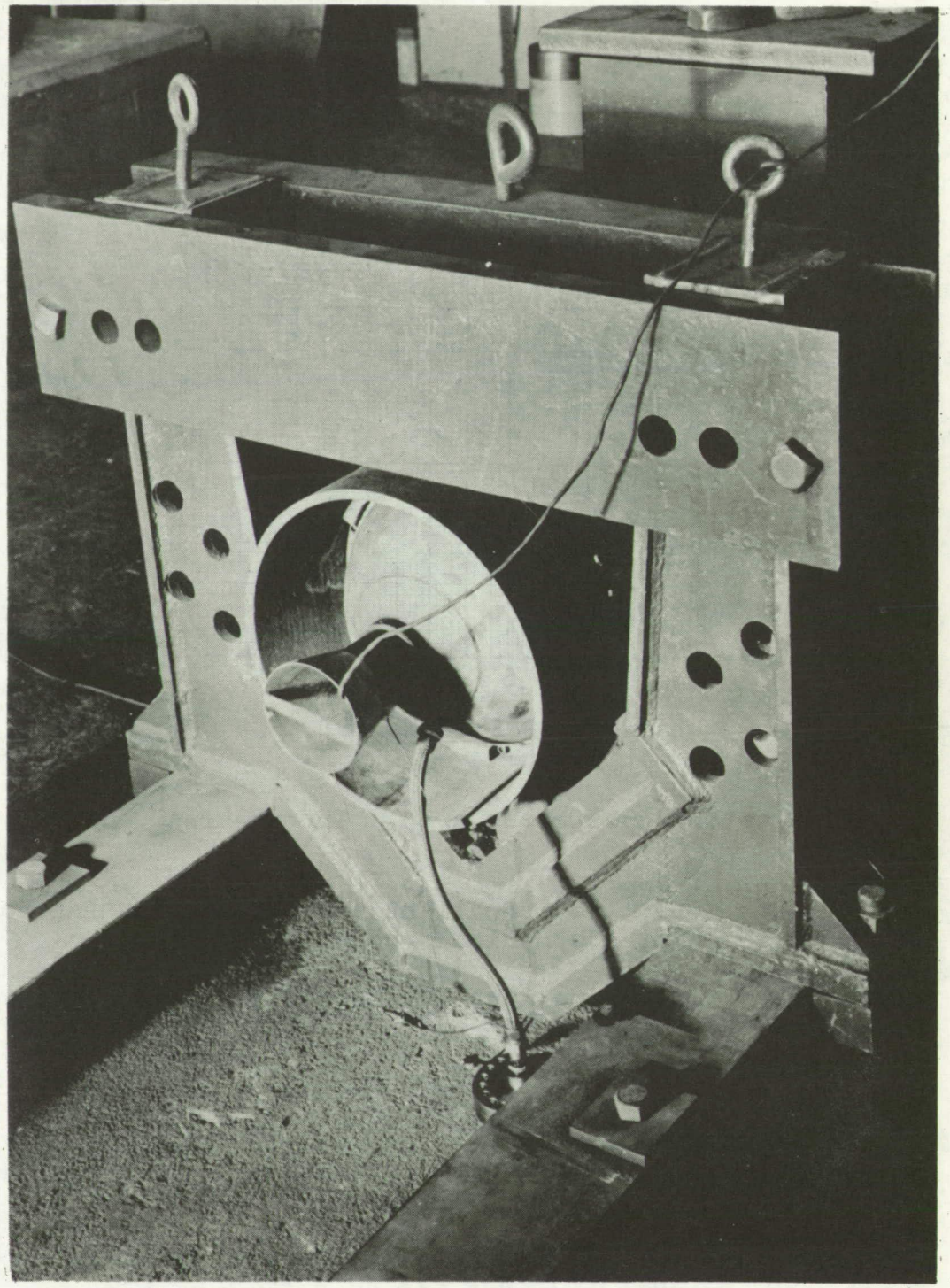

L-57-1921

Figure 10.- Spherical-rocket-motor mount for static tests.

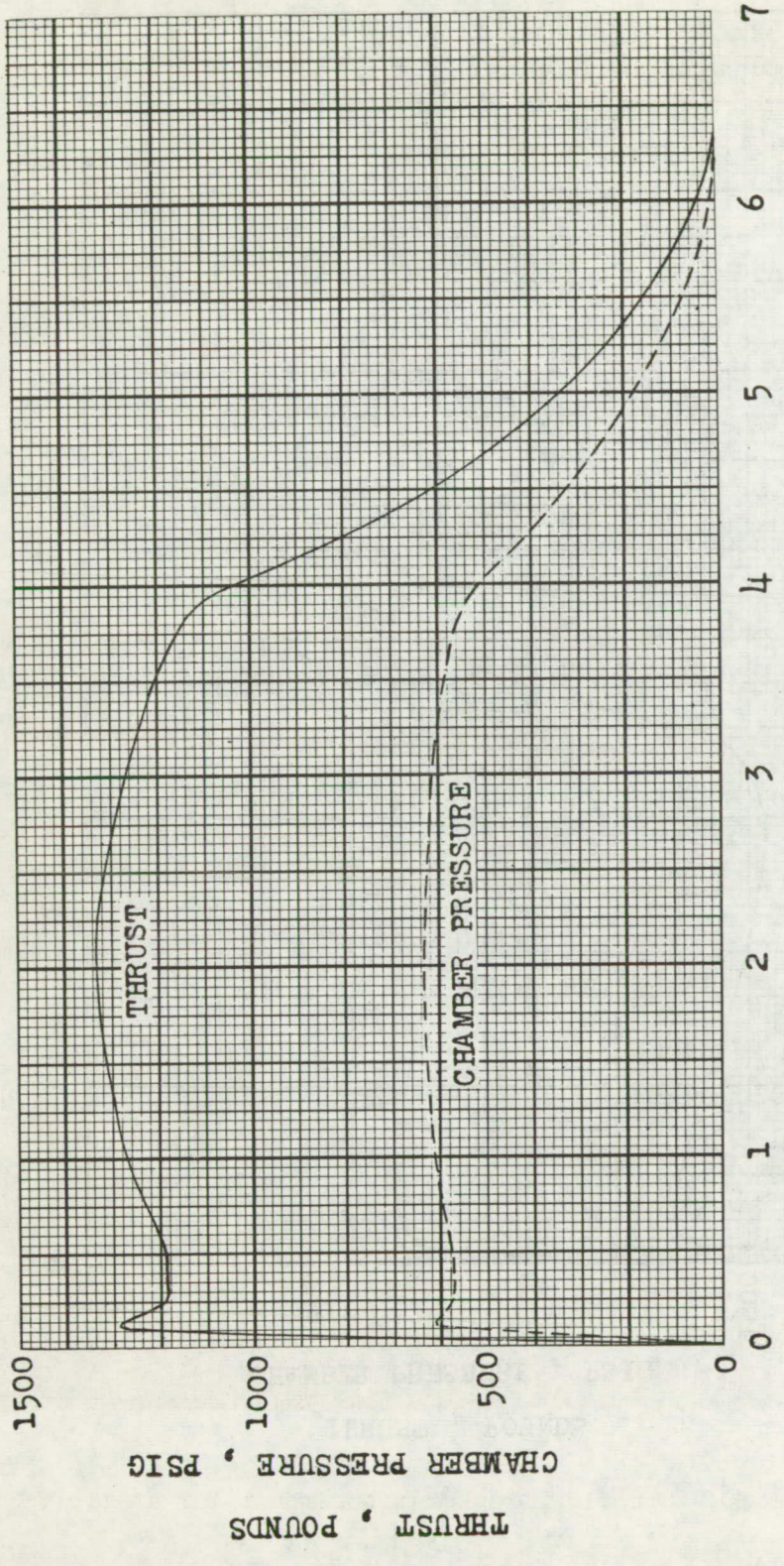

Figure 11.- Performance of spherical rocket 1.

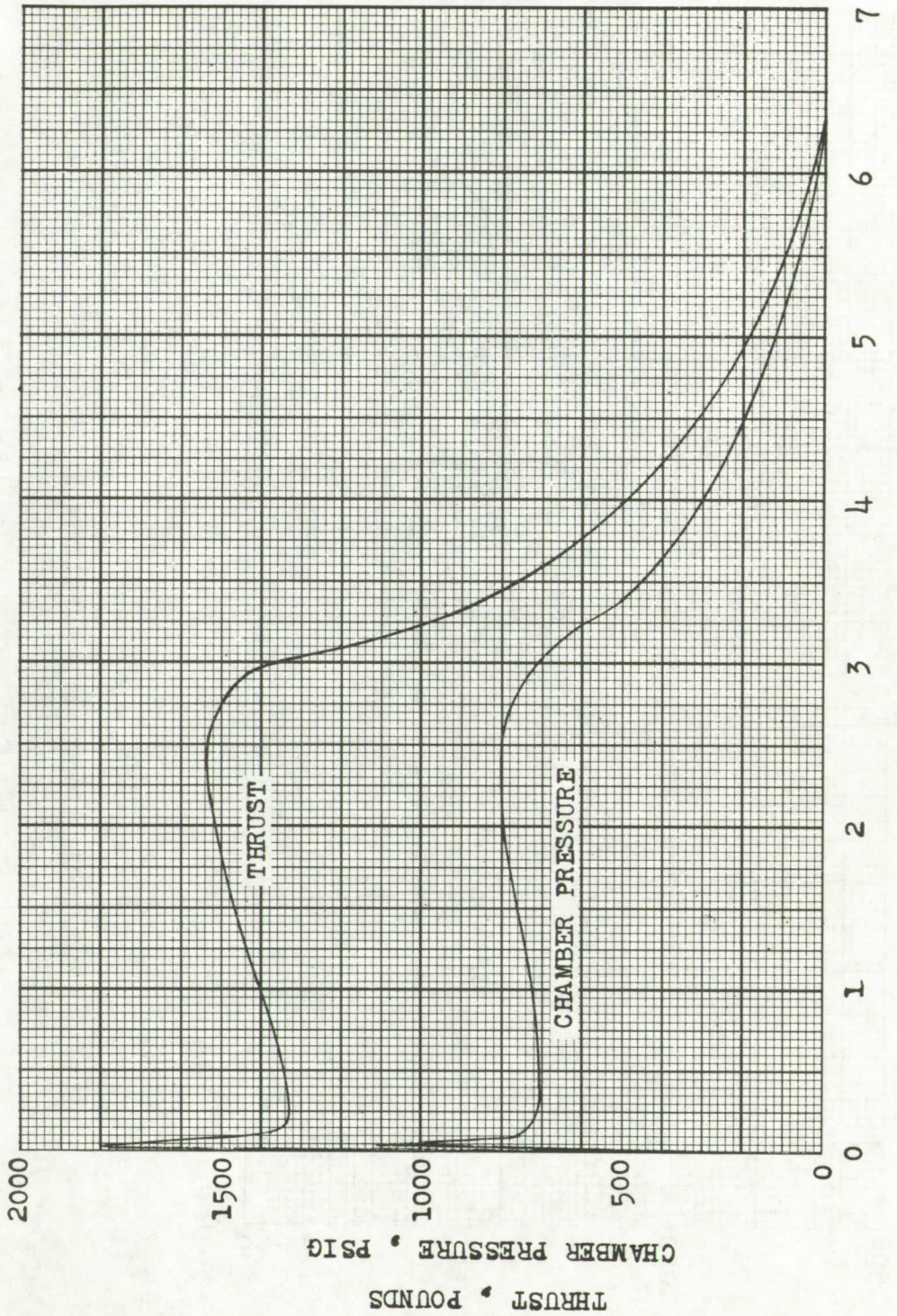

Figure 12.- Performance of spherical rocket 2.

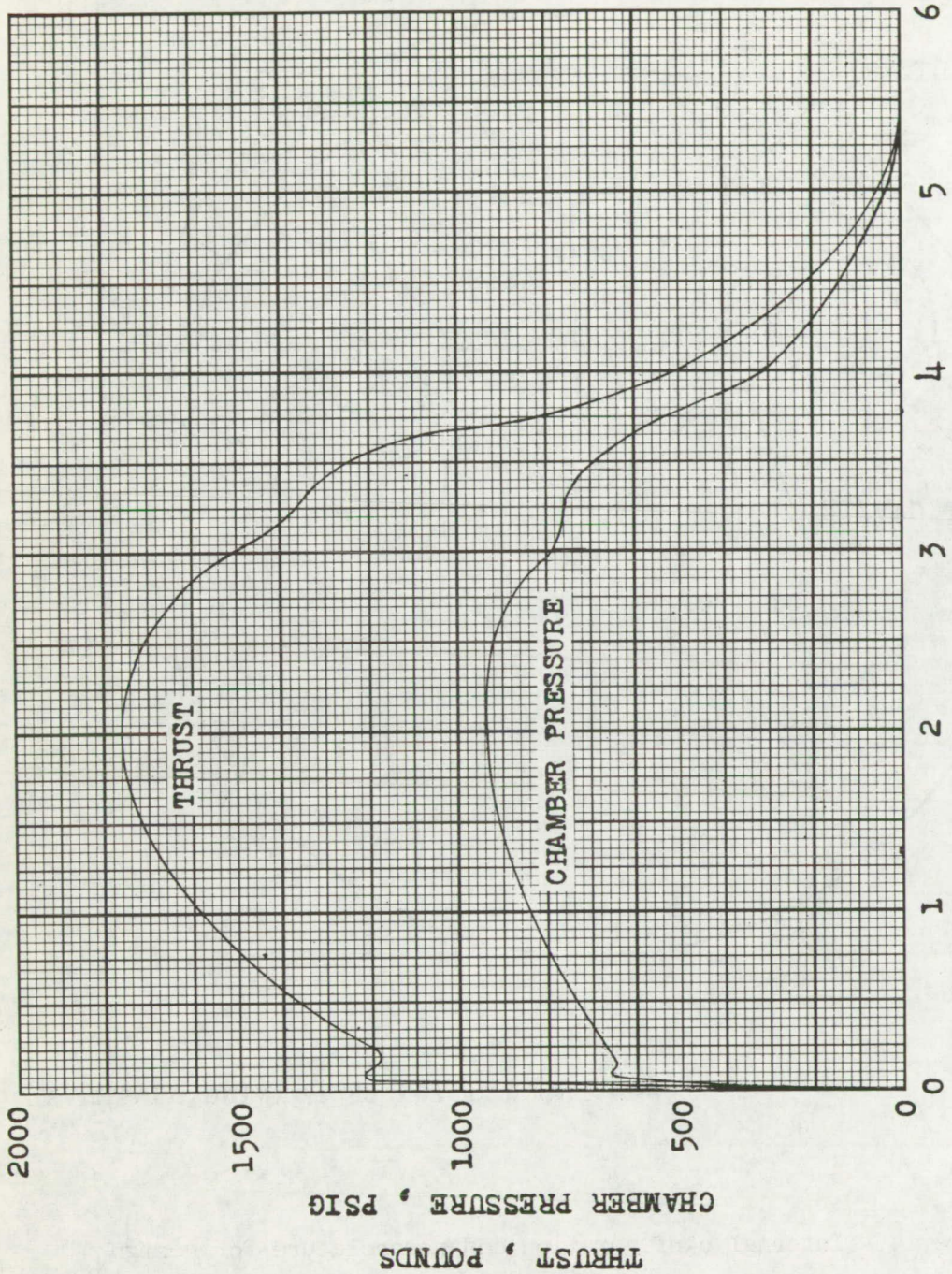

Figure 13.- Performance of spherical rocket 3.

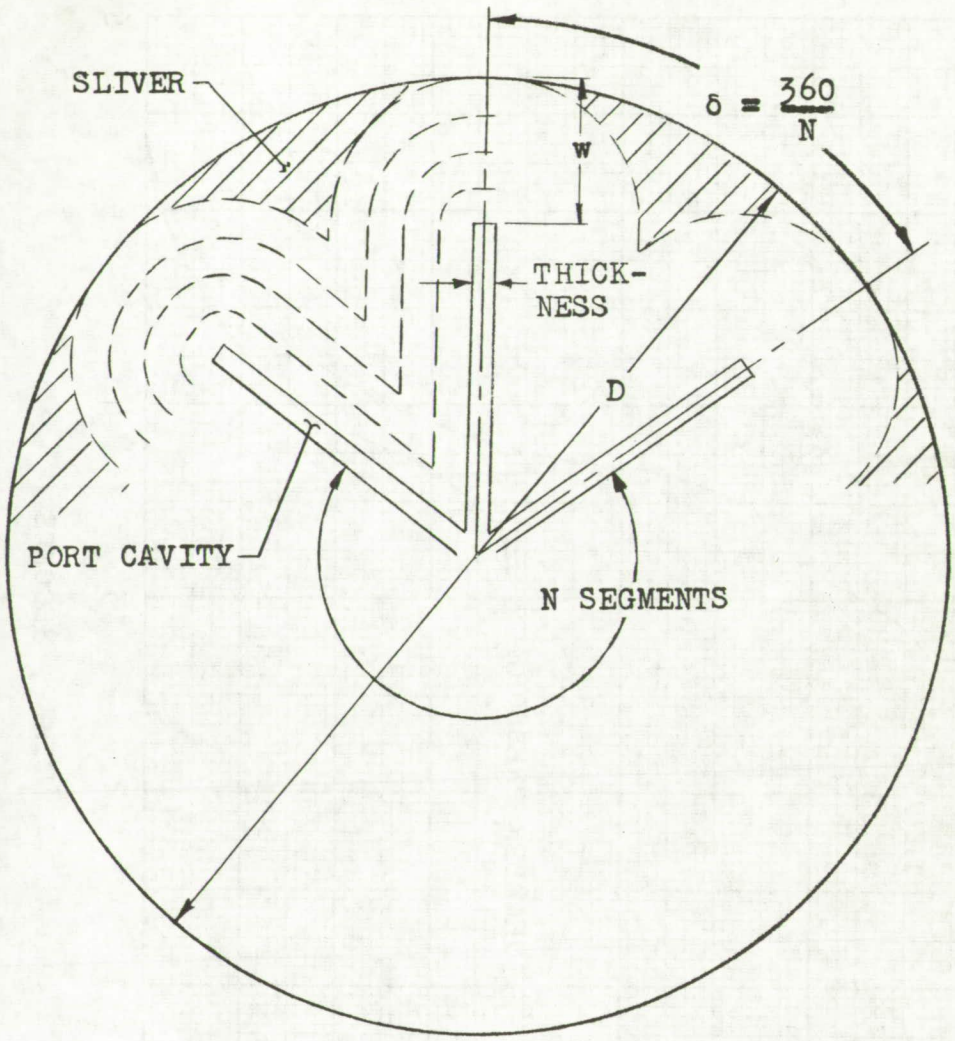

Figure 14.- Internal configuration and nomenclature for design calculations.

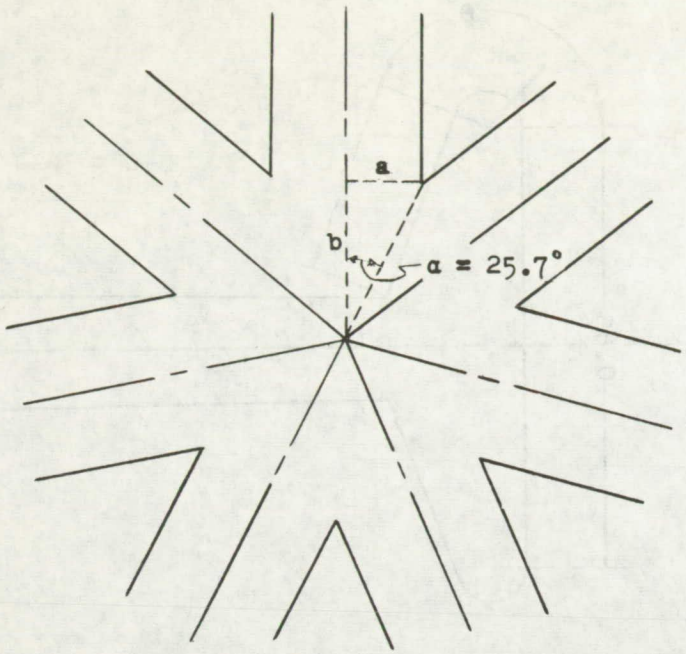

(a) Polar-surface geometric characteristics.

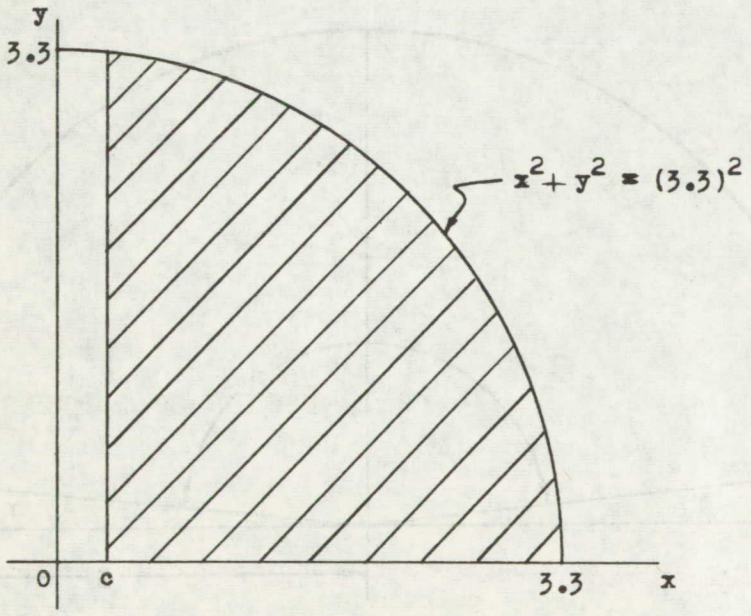

(b) Facial-area geometric characteristics.

Figure 15.- Surface-area calculation sketches.

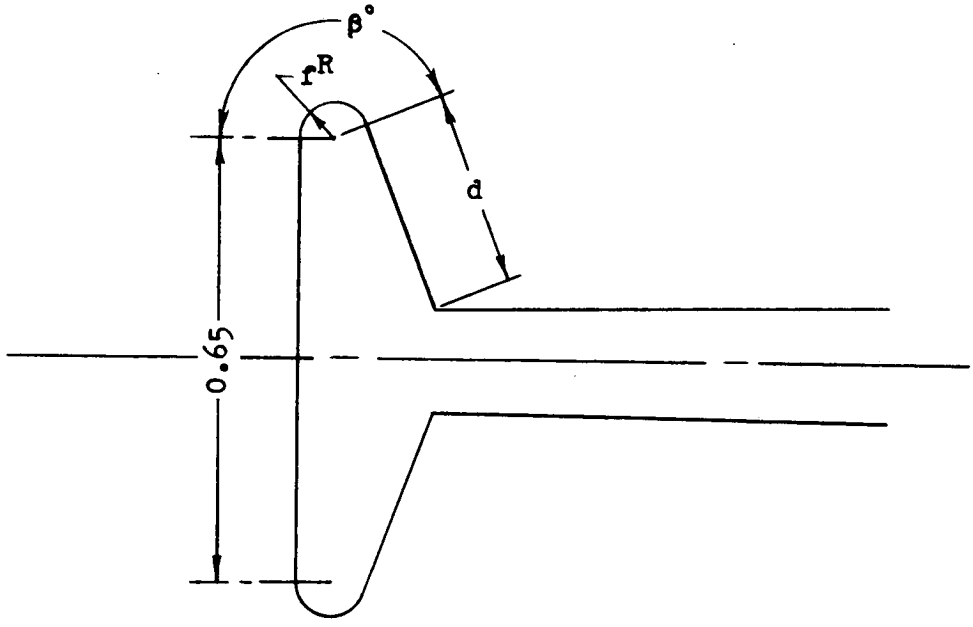

(c) Tee-flare geometric characteristics.

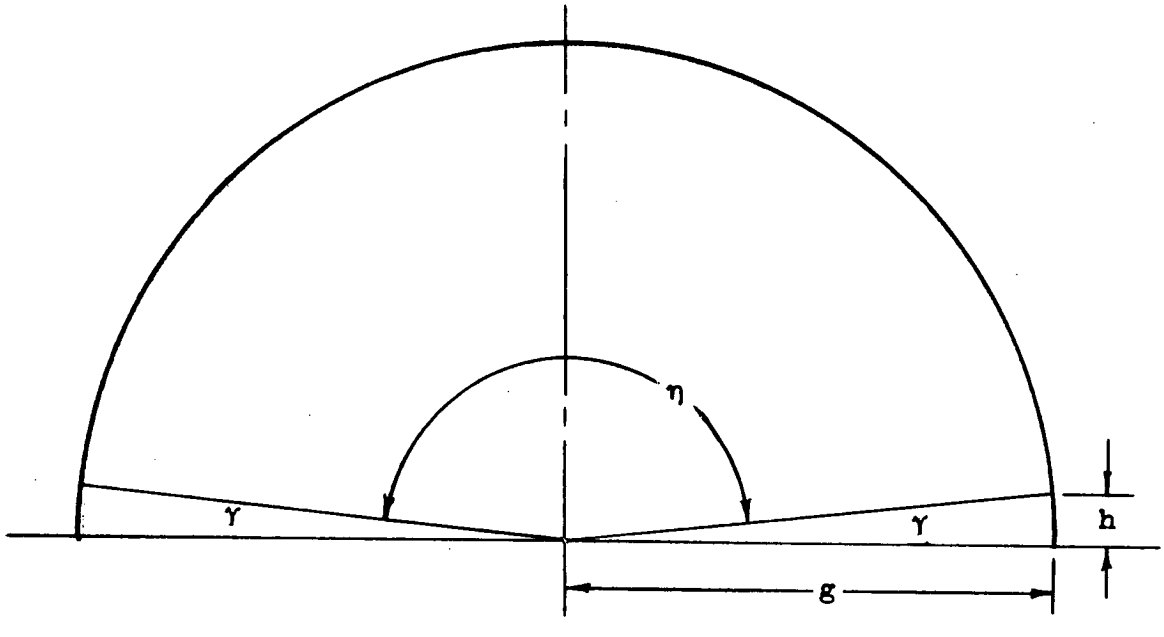

(d) Perimeter geometric characteristics.

Figure 15.- Concluded.